Bethe lattice approach and relaxation dynamics study of spin-crossover materials

Toussaint Djidjoho Oke, Félix Hontinfinde & Kamel Boukheddaden

Applied Physics A
Materials Science & Processing

ISSN 0947-8396

Appl. Phys. A
DOI 10.1007/s00339-015-9189-x

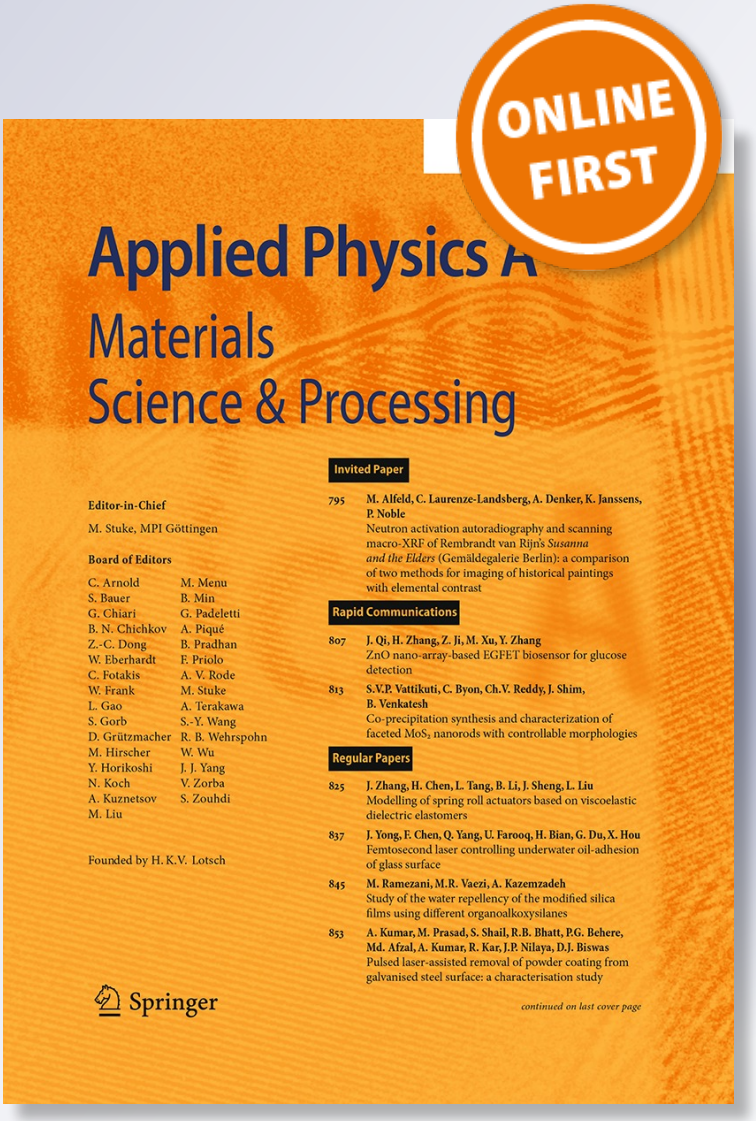

Springer

Appl. Phys. A
DOI 10.1007/s00339-015-9189-x

Applied Physics A
Materials Science & Processing

Bethe lattice approach and relaxation dynamics study of spin-crossover materials

Toussaint Djidjoho Oke[1] · Félix Hontinfinde[1] · Kamel Boukheddaden[2]

Received: 22 November 2014 / Accepted: 20 April 2015

Abstract Dynamical properties of Prussian blue analogs and spin-crossover materials are investigated in the framework of a Blume–Emery–Griffiths (BEG) spin-1 model, where states ± 1 and 0 represent the high-spin (HS) state and the low-spin state, respectively. The quadrupolar interaction depends on the temperature in the form $K = \alpha k_B T$. Magnetic interactions are controlled by a factor $\gamma = J/K$ such that for $\gamma = 0$ ($J = 0$), magnetic ordering is not expected. The model is exactly solved using the Bethe lattice approach for the equilibrium properties. The results are closer to those calculated by numerical simulations with suitable Arrhenius-type transition rates. The study of relaxation processes of non-equilibrium HS states revealed one-step nonlinear sigmoidal relaxation curves of the HS fraction at low temperatures. We found that increasing the magnetic interactions leads to the appearance of a plateau in the thermal hysteresis as well as in the relaxation curves of the HS fraction at low temperature.

✉ Félix Hontinfinde
fhontinfinde@yahoo.fr

Toussaint Djidjoho Oke
adedjim@gmail.com

Kamel Boukheddaden
kamel.boukheddaden@yahoo.fr

[1] Département de Physique (FAST) et Institut des Mathématiques et de Sciences Physiques (IMSP), Université d'Abomey-Calavi, 01 BP 613 Porto-Novo, Benin

[2] Groupe d'Etudes de la matière condensée, Université de Versailles/St. Quentin en Yvelines-CNRS, 45 Avenue des Etats Unis, 78035 Versailles Cedex, France

1 Introduction

In recent years, a particular importance was attached to the field of spin-crossover (SC) materials because of their potential applications in memories, sensors, switches, and display devices. For that purpose, the cooperative phenomena where both SC and magnetic ordering are involved have been studied intensively [1–5]. These materials are particularly interesting because under various constraints such as temperature, pressure, magnetic field, and light, phase transitions between the low-spin (LS) diamagnetic state and a high-spin (HS) paramagnetic state should occur [6–8]. The change of the system thermal energy during the spin-state transition leads to both electronic and structural changes, often observed as a color and/ or magnetic moment change [1, 9]. When the interaction between molecules is weak, the HS fraction changes smoothly with temperature, whereas when it becomes strong, the system exhibits cooperative phenomena [10]. Then, the change in HS fraction becomes sharper and sharper with increasing SC interactions strength. Of course, the interaction in SC solids is purely due to the volume increase subsequent to the metal–ligand distance expansion, which itself is the result of the redistribution of the electrons between the bonding t_{2g} and the antibonding e_g orbitals. In the diamagnetic ($S = 0$) LS state, only bonding orbitals are populated ($t_{2g}^6 e_g^0$), while in the paramagnetic ($S = 2$) HS state, the electronic configuration becomes ($t_{2g}^4 e_g^2$). Obviously, the elastic interactions are at the hearth of the existence of cooperative effects in SC materials, and so they play a crucial role in the existence of the first-order transitions and the thermally induced hysteresis loops observed experimentally. From the experimental point of view, it is established that the SC transition involves both electronic

Published online: 05 May 2015

transformation (spin and orbital) and structural modifications [11–14].

Theoretically, many interesting works have addressed transitions in both static and dynamic properties of SC transitions. Most of them are based on Ising-like models [15–17], or more realistic descriptions, using elastic models [18–20] or atom–phonon coupling models [9, 21, 22]. They are accompanied by Monte Carlo simulations [23–25] or method of molecular dynamics [26]. In the work [27], it was found that Ising-like model is equivalent to Blume–Emery–Griffiths (BEG) Hamiltonian with degenerate levels. More recently, a BEG model with spin–phonon interactions has been introduced and studied by corrective effective field theory (CEFT) and Monte Carlo simulations for spin-crossover materials [28]. There, the quadrupolar coupling parameter K is assumed to depend linearly on the absolute temperature T in the form, $K = \alpha K_B T$. The effective ligand-field strength D depends on the absolute temperature, the degeneracy ratio between LS and HS states and the ligand-field strength. In the present work, we consider the previous model that we solve exactly within the Bethe-Peierls approximation. The model is defined on the Bethe lattice, which is a recursive graph. The exact recursion relations obtained are solved numerically, and different results are compared with those obtained in the previous work. On the other hand, dynamical properties of the model are computed by using Monte Carlo simulations (MCS) [29, 30] with suitable Arrhenius transition rates [31, 32]. These dynamics have been proven efficient in reproducing qualitatively and quantitatively experimental data [33–35]. The relaxation of HS fraction shows typical sigmoidal shapes, associated with one-step relaxations [33, 34, 36].

The paper is organized as follows. Section 2 is devoted to the presentation of the model and a description of the used calculation methods: Bethe Approximation (BA) and Monte Carlo algorithm. In Sect. 3, we present and discuss the obtained results. Section 4 contains the conclusion.

2 Model and methods

2.1 The model Hamiltonian

Following reference [28], the Hamiltonian of the spin-1 BEG model that is considered reads:

$$H = -J \sum_{\langle i,j \rangle} s_i s_j - K \sum_{\langle i,j \rangle} s_i^2 s_j^2 + D \sum_i s_i^2 - h \sum_i s_i, \qquad (1)$$

where each spin $s_i = 0, \pm 1$ is located at a site i of the lattice, $\langle i,j \rangle$ indicates nearest neighbors (NN) pairs. The first sum is over the interacting nearest neighbors, J denotes the magnetic interaction parameter. The parameters K and D are the quadrupolar interaction constant and the effective ligand-field strength, respectively. h is an external magnetic field that acts one the system. The Zeeman effect [37] is considered in the model [27] with the presence of an external field h. In the model, $s = 0$ denotes the non-magnetic low-spin state, while $s = \pm 1$ corresponds to the magnetic high-spin state. Degeneracies of non-magnetic and magnetic states are different. Actually, the spin states are fictitious spin states and not true spins. In fact, the spin value $s = 0$ is affected to the LS state and the spins $s = \pm 1$ are associated with the HS state. In the problem, the degeneracy ratio g of the true spin is included in the ratio of the effective degeneracies between the HS and the LS states [28]. The degeneracy ratio g originates from the difference in the molar entropy between LS and HS states. The parameter g depends on the temperature through the phonon density of the lattice. In the following, it is taken as a constant.

In the model, $K = \alpha k_B T$; $D = \Delta - k_B T \ln(g)$ represents the effective difference of the crystal fields in the LS and the HS states. More precisely, Δ corresponds to the difference of ligand-field energies between the two spin states. The D parameter is indeed written so as to favor the LS state at low temperature. The HS state, which appears at high temperatures where the lattice is softer, needs thermal excitations, which have been taken into account in the quantity $-k_B T \ln(g)$ which enters in "the ligand field energy" as an effective contribution to D, reflecting the entropic effects. In a more elaborate model, D depends both on the true ligand-field and the elastic intermolecular interaction strengths as demonstrated in Ref. [27]. Here, the transition temperature in the absence of magnetic field and magnetic interactions is given by $T_{1/2} = \Delta / k_B \ln(g)$. Within the used parameter values, $\Delta = 400$ K and $g = 100$, the obtained transition temperature is ~ 86 K. However, in true PBA compounds, which can be photo-excited until ~ 100 K, the transition temperatures are ranged between 240 and 300 K [38–42]; so our energy gap between the LS and the HS states is pretty small. In this work, we are mostly interested in the out of equilibrium properties of PBA, like the relaxation of photo-induced metastable HS states and how their time dependence is affected by the magnetic interactions. Changing Δ value will not change the qualitative behavior of the obtained results. The model is solved using two well-known methods of statistical mechanics: the Bethe lattice approach [43] and Monte Carlo Simulations based on Arrhenius dynamics [33–35].

2.2 The Bethe lattice approach formulation

A Bethe lattice is a regular tree, i.e., a connected graph without circuits. Historically, it takes its name from the fact that its partition function is exactly that of an Ising model in the Bethe approximation [43]. In the past, the Bethe lattice has been widely used in solid state and statistical physics for modeling various systems because of its

recursive and uniform structure. It often reflects the essential features of spin models when the conventional mean field approach failed [44–48]. It consists of a central spin s_0 which may be called the first-generation spin. This spin has a number z of nearest neighbors, which form the second-generation spins. Each site of the second generation is joined to $z-1$ nearest neighbors. Thus, the second generation has $z(z-1)$ nearest neighbors, which form the third generation and so on to infinity as shown in Fig. 1.

In order to calculate the order parameters, one first uses the partition function given by [49]:

$$Z = \sum \exp(-\beta H) = \sum_{\mathrm{Spc}} P(\mathrm{Spc}) \tag{2}$$

where $P(\mathrm{Spc})$ can be thought of as an unnormalized probability distribution over the spin configuration and $\beta = 1/k_B T$. If the Bethe lattice is cut in some central point with a spin s_0, spin of type s, then it splits up into z identical branches, i.e., disconnected pieces. Each of these is a rooted tree at a central spin s_0. This implies that $P(s_0)$, with $\mathrm{Spc} = s_0$ of a spin configuration with the spin value s_0 at the central site, can be written as :

$$P(s_0) = \exp[\beta(-Ds_0^2 + hs_0)] g_n^z(s_0). \tag{3}$$

Similarly,

$$P(s_1) = \exp[\beta(-Ds_1^2 + hs_1)] g_{n-1}^z(s_1). \tag{4}$$

Now we define :

$$g_n(s_0) = \sum_{s_1} \exp\left[\beta(Js_0s_1 + Ks_0^2 s_1^2 - Ds_1^2 + hs_1)\right] \times [g_{n-1}(s_1)]^{z-1}, \tag{5}$$

$$g_{n-1}(s_1) = \sum_{s_2} \exp\left[\beta(Js_1s_2 + Ks_1^2 s_2^2 - Ds_2^2 + hs_2)\right] \times [g_{n-2}(s_2)]^{z-1} \tag{6}$$

where

$$g_n(s_0) = g_{n-1}(s_1). \tag{7}$$

Hence,

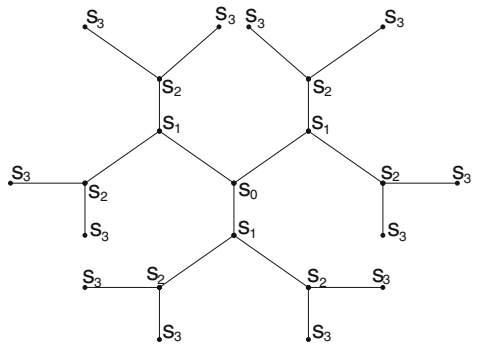

Fig. 1 A Bethe lattice with sites of coordination number $z = 3$

$$P(s_0) = P(s_1).$$

As an example, the calculation of $g_n(s_0)$ yields

$$g_n(\pm 1) = \exp[\beta(\pm J + K - D + h)][g_{n-1}(1)]^{z-1} + \exp[\beta(\mp J + K - D - h)][g_{n-1}(-1)]^{z-1} + [g_{n-1}(0)]^{z-1}, \tag{8}$$

$$g_n(0) = \exp[\beta(-D + h)][g_{n-1}(1)]^{z-1} + \exp[-\beta(D + h)][g_{n-1}(-1)]^{z-1} + [g_{n-1}(0)]^{z-1}. \tag{9}$$

The recursion relations are obtained from the ratios of the g_n functions for spin-1 as follows:

$$X_n = \frac{g_n(+1)}{g_n(0)}, \quad Y_n = \frac{g_n(-1)}{g_n(0)} \tag{10}$$

$$X_{n-1} = \frac{g_{n-1}(+1)}{g_{n-1}(0)}, \quad Y_{n-1} = \frac{g_{n-1}(-1)}{g_{n-1}(0)}. \tag{11}$$

From Eqs. (7), (10), (11), it follows:

$$X_n = X_{n-1}, \quad Y_n = Y_{n-1}. \tag{12}$$

Now, we can calculate the magnetization (m) and the quadrupolar moment ($n_{HS} = q$ fraction) on the lattice,

$$m = Z_1^{-1} \sum_{s_0} s_0 P(s_0), \quad q = Z_1^{-1} \sum_{s_0} s_0^2 P(s_0) \tag{13}$$

After some calculations, we obtain :

$$m = \frac{\exp[\beta(-D + h)] X_n^z - \exp[-\beta(D + h)] Y_n^z}{1 + \exp[\beta(-D + h)] X_n^z + \exp[-\beta(D + h)] Y_n^z}, \tag{14}$$

$$q = \frac{\exp[\beta(-D + h)] X_n^z + \exp[-\beta(D + h)] Y_n^z}{1 + \exp[\beta(-D + h)] X_n^z + \exp[-\beta(D + h)] Y_n^z}. \tag{15}$$

Then, the phase diagrams for a given coordination number z are obtained by studying the thermal variations of the order parameters. The most common phase transitions are of second order and first order type for most systems. The second order phase transition temperature, T_c, is the temperature at which the total magnetization goes to zero continuously. In order to calculate the first-order phase transition temperatures, we need the analysis of the free energy expression $F = -k_B T \ln Z$ which is given in terms of the recursion relations by:

$$F = -\frac{1}{\beta}\left[\frac{z-1}{2-z}\ln A + \frac{1}{2-z}\ln A + \ln B\right], \tag{16}$$

where

$$A = \exp[\beta(-D + h)] X_n^{z-1} + \exp[-\beta(D + h)] Y_n^{z-1} + 1$$

and

$$B = \exp[\beta(-D + h)] X_n^z + \exp[-\beta(D + h)] Y_n^z + 1.$$

In the thermodynamic limit, (X_n, Y_n) converges to the fixed point (X_s, Y_s). In this case, substituting X_s, Y_s in Eqs. (14)–(15), one obtains :

$$m = m(X_s, Y_s); \quad q = q(X_s, Y_s).$$

Numerically, multiple solutions of (X_s, Y_s) may exist. The stable solution is obtained from the minimum value of the free energy. Others correspond to unstable or metastable states. The substitution of the stable solution (X_s, Y_s) into the expressions of m, q and F yields their true values.

2.3 Dynamical aspects

Upon thermal fluctuations, several dynamics with microscopic transition rates could be considered for the study of spin-crossover materials [31, 35, 50]. Among them, the Arrhenius and Glauber dynamics are indicated. Following [33, 34], we consider $P(\{s\}, t)$ as the probability of observing the system in the configuration $\{s\} = (s_1, ..., s_N)$ at time t. This probability evolves in the course of the time following the master equation:

$$\frac{\partial P(\{s\}, t)}{\partial t} = -\sum_{j=1}^{N} W_j(s_j \to s_j') P(\{s\}_j, s_j, t) + \sum_{j=1}^{N} W_j(s_j' \to s_j) P(\{s\}_j, s_j', t) \tag{17}$$

where $\{s\}_j$ denotes the configuration of all spins excepted spin s_j, $W_j(s_j \to s_j')$ the probability per unit time for transition from the configuration $\{s\}_j$ to $\{s'\}_j$. $W_j(s_j \to s_j')$ and $W_j(s_j' \to s_j)$ may fulfill the detailed balance condition at equilibrium (see Refs. [31, 32]). $W_j(s_j \to s_j')$ is chosen proportional to $\exp(-\beta E_j)$, where $E_j = -Js_j \sum_i s_i - Ks_j^2 \sum_i s_i^2 + Ds_j^2 - hs_j$. Spins s_i are nearest neighboring spins of spin s_j.

In spin-crossover problems, the transition between the molecular LS and HS states takes place over an energy barrier that originated from the strong vibronic coupling inside molecules [18, 51]. Obviously, the local volume change is due to occupation of e_g (antibonding) orbitals, which leads to 10 % [27] increase in the metal–ligand distance at least for Fe(II) SC compounds, while for Fe(III), this expansion is much smaller, due to the weakness of the vibronic interaction strength between the electronic and the vibrational degrees of freedom inside the molecule. However, the global volume change of the lattice in a cooperative way, i.e., in a very narrow temperature interval, is clearly due to the elastic interactions. The elasticity, combined with the local volume changes, produces a cooperative global volume change, which in turn generates a mechanical lattice instability when the system reaches some threshold temperature (in the way LS/HS transition) at which the LS state becomes unstable [51–54].

For the simulations, the standard Monte Carlo algorithm [29, 30] is used. The simulation propagates as follows. An initial spin configuration of the system is chosen. The evolution of this configuration is attempted on a randomly selected site j. Then, the energy E_j is calculated. Due to the three spin states of the system, the transition probability is taken in the form (see Refs. [33, 34, 55]):

$$W_j(s_j \to s_j') = \frac{1}{3\tau} \mathrm{e}^{-\beta E_j} \tag{18}$$

where $1/\tau$ denotes the effective intramolecular frequency associated with the "spontaneous spin reversals," which provides the time scale of the dynamics.

According to the thermal activation spin-flip process, it depends on the temperature as follows:

$$\frac{1}{\tau} = \frac{1}{\tau_0} \mathrm{e}^{-\beta E_0^a}, \tag{19}$$

where $1/\tau_0$ is the "intrinsic" frequency spin-flip process between HS/LS states taken as constant and E_0^a denotes the intramolecular vibronic energy barrier.

In the following, τ_0 is set to 500 s. After that, a random number $0 \le r \le 1$ is chosen and the spin-flip move is accepted with the calculated probability $W_j(s_j \to s_j')$. The obtained configuration is submitted for the second simulation step. After a suitable number of Monte Carlo moves n_{MC} found to be about $2 \times 10^3 L^2$ Monte Carlo steps (MCS) where L is the system size, stationary values of physical quantities of interest are calculated using a statistical averaging procedure. Thus, the n_{HS} fraction is given by:

$$n_{\mathrm{HS}} = L^{-2} \sum_s n(\pm)_s, \tag{20}$$

where $n(\pm)_s = n(+)_s + n(-)_s$ and $n(+)_s/n(-)_s$ denote the number of up/down spins of the configuration $\{s\}$. For the magnetization, $n(\pm)$ in the previous formula is replaced by $n(+) - n(-)$.

3 Results and discussions

3.1 Metastable states and phase diagrams

First, α and γ are set to zero in Eq. (1). The high-spin fraction n_{HS} becomes then the key order parameter of the system. Equations (14) and (15) have been solved numerically. In Fig. 2a, we display results on n_{HS} calculated using the recursion relations as a function of the absolute temperature for varying values of the parameter α and for selected values of g and Δ. For increasing values of α, the HS state is stabilized as found in reference [28]. At low values of α, n_{HS} continuously increases with temperature.

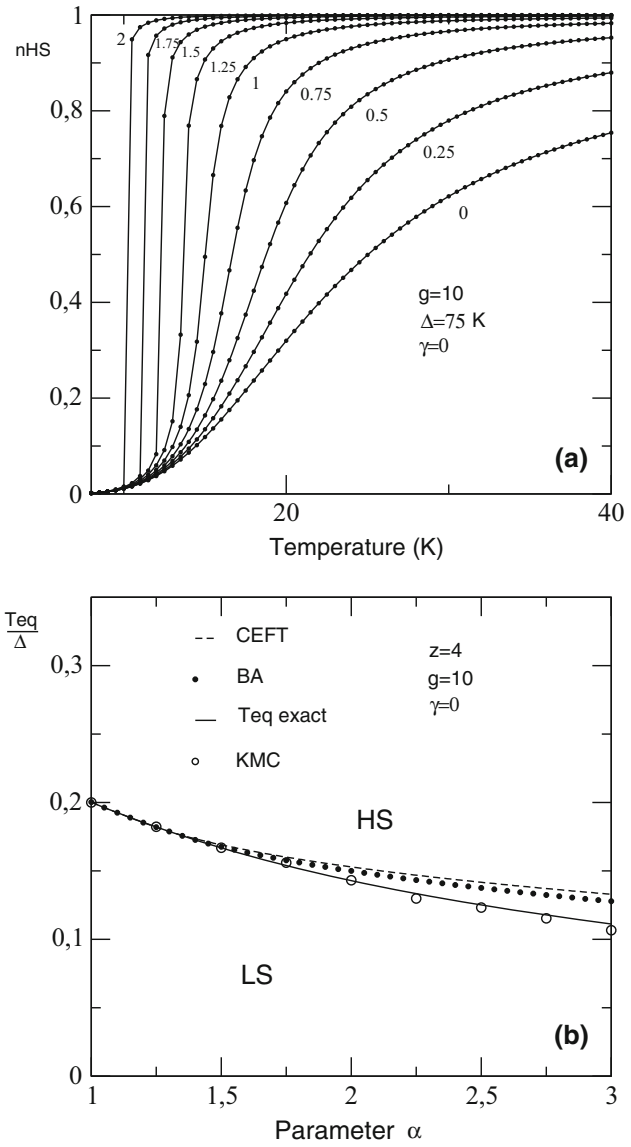

Fig. 2 Thermal behaviors of the high-spin fraction n_{HS} for some selected values of the model parameters (**a**). Jumps appear in the *curves* for $\alpha \geq 1.25$. In (**b**) results by Bethe Approximation are compared with those from reference [28]. The results appear better than those by CEFT [28]. Different *curves* in (**b**) are obtained by solving numerically the equation $n_{HS} = 1/2$

For large values of α associated with cases of high contribution of spin–phonon interactions and lattice elastic constants, the HS state is reached through a jump in the behavior of the n_{HS}. Therefore, the transition is of first order. The latter becomes sharper and sharper as the quadrupolar parameter α increases. It then appears that, the spin transition occurs either by a continuous transition or through a first-order transition. As observed in several previous works, n_{HS} increases and tends to the value 1 at high temperature. The equilibrium temperature T_{eq} is obtained when both HS and LS states are equipopulated, i.e., $n_{HS} = 1/2$.

In Fig. 2b, we compare results obtained by CEFT (dashed line) [28], KMC (open circles) [28] and by an exact mapping of the model onto the WP model in the previous work [28] with those by the Bethe approximation (dotted line). The Bethe lattice approach generates results that look better than those by CEFT. Above the transition lines, the system lies in the *HS* state with magnetically disordered configurations, and below, the diamagnetic phase prevails.

In Fig. 3, we show the validity limits of the Bethe lattice approach scheme by comparing its results in the absence of magnetic ordering with those obtained through exact calculations by a mapping of the system onto a WP model [15]. It emerges that higher are the coordination number z and interactions in the model, more important are discrepancies between both results. In the following, we restrict our calculations to low values of z, say 3 and 4.

Now, let us study the influence of the Zeeman effect on the spin transition. From Fig. 4a, one notices that for $\alpha = 0$, increasing h just shifts the n_{HS} curve to the low-temperature region. This situation decreases the spin-transition temperature and stabilizes the HS state. At constant h (e.g., $h = 40$), increasing α still have the same effect on the system. It leads the continuous spin transition to a sharp

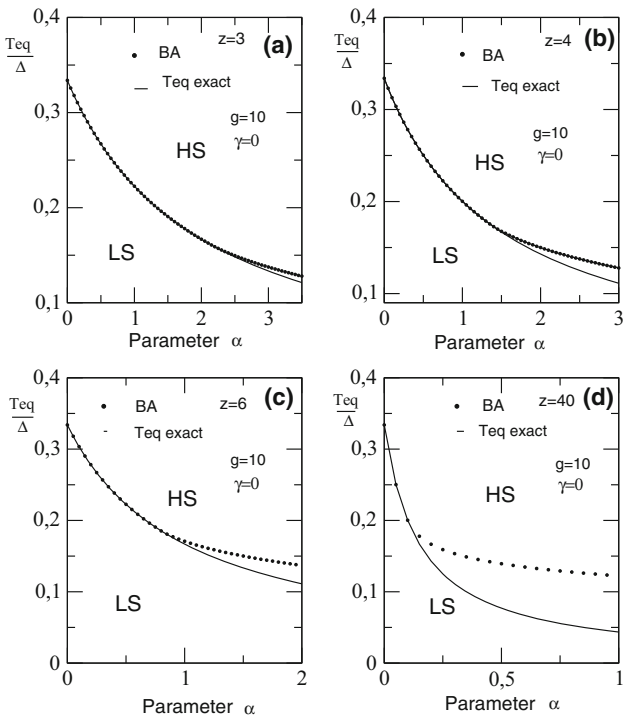

Fig. 3 Finite-temperature phase diagrams in the (α, T_{eq}/Δ) plane by two different methods: BA (*closed circles*) and exact calculations [28] (*line*; see text) for $g = 10$, $\gamma = 0$. **a** $z = 3$; **b** $z = 4$; **c** $z = 6$; **d** $z = 40$ and selected values of z. Higher are the coordination number z and spin–phonon interactions in the model, more important are discrepancies between results by both methods

first-order transition. Figure 4b shows clearly that T_{eq} is a decreasing function of h at constant Δ. Accordingly, the volume of the HS state increases under the Zeeman effect. This property may be of high technological use. The exact free energy [56–58] of the system is calculated for some selected values of h (Fig. 4c) and Δ (Fig. 4d) as a function of α. The corresponding curves show in both panels, the existence of a fixed point. An analysis of this crossing point which is associated with $F = 0$ indicates that it corresponds to the onset of first-order transitions in the model. Surprisingly, this onset is independent of Δ and h. Trends of different results show that when h decreases or Δ increases, the diamagnetic phase has less and less magnetic species spins -1 or $+1$ and the LS state is stabilized.

In the following, HS units are considered to interact magnetically in the system. Phase boundaries are determined, and corresponding phase diagrams constructed (Fig. 5). The second-order phase boundaries are obtained when the total lattice magnetization vanishes. At the first-order transition temperatures, both m and q show discontinuities in their behaviors. The positions of the TCP differ slightly from those found by CEFT in reference [28] and indicate the existence of tricritical lines. Both methods yield similar temperature phase diagrams.

3.2 Non-equilibrium relaxation paths

In view to derive dynamical properties of the system, the numerical simulation procedure described above with Arrhenius dynamics is considered to solve the kinetic equation of the system. These dynamics have been proven efficient in studying relaxation processes for HS $\leftrightarrow$ LS spin-flip [31]. A sample of size $L = 100$ is considered. The individual spin-flip rate between the HS and LS states is fixed to $2 \times 10^{-3}\mathrm{s}^{-1}$. The generated results on the thermal evolution of the HS fraction with thermal fluctuations are compared with those by BA. The observed agreement looks interesting. One should, however, notice that due to the absence of short-range correlations in the analytical approach in the low-temperature range, the results should only coincide in the high temperature regime. In the calculations, the intramolecular energy barrier E_0^a is set to zero in equation (19). As in previous works, at high temperature, n_{HS} tends to 1.

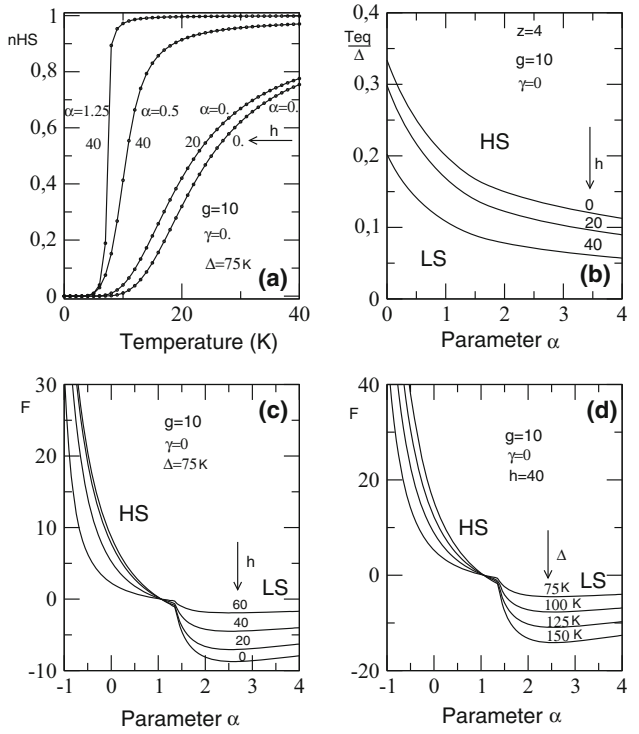

Fig. 4 Some features of the model as functions of the temperature and the parameter α. **a** Effect of α and h on the n_{HS} fractions at fixed other parameters. The external field h stabilized the HS phase. Similar effect was observed with increasing values of α (see Fig. 2a). **b** T_{eq}/Δ as function of α at selected values of h. In (**c**) the behavior of the system free energy F is given as a function of α for selected values of h and $\Delta = 75$ K. In (**d**), F is plotted against α for selected values of Δ for $h = 40$

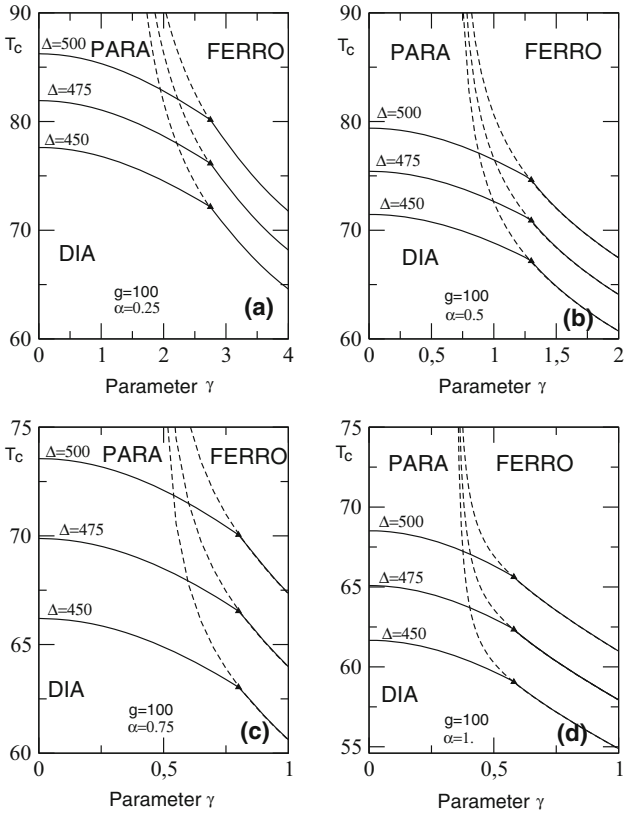

Fig. 5 Thermal phase diagrams by the BA method in the (T_c, γ) plane for different values of Δ and α. Three phases are found. *Dashed lines* are critical lines. *Triangles* denote tricritical points (TCP). Their positions seem not to depend on Δ. At the right-hand side of the TCP, transitions are of first order

As previously demonstrated by several authors [1, 9], structural/electronic cooperativity may sometimes give bistability. In other words, at the vicinity of the first-order transition, thermal hysteresis loop may be detected. To check that, and precisely find the onset of the first-order transitions, we heated the system sequentially from $T = 25$ K to $T = 40$ K with a temperature step $\Delta T = 0.1$ K and cooled it down to $T = 25$ K. For the appearance of the hysteresis loop, the equilibrium temperature T_{eq} must be smaller than the critical temperature of the corresponding pure Ising model [27, 55]. One gets, as displayed in Fig. 6b, a symmetric hysteresis loop. By comparing the loop obtained by MC simulations with the one derived by BA, one sees a remarkable agreement. The transition temperatures are in the range of 36.05 and 36.60 K for the upward branch, 27.6 and 27.40 K for the downward one, respectively. The corresponding ratio of the width of the thermal hysteresis loop by the two methods is about 0.92 which is very close to 1. This shows the accuracy of the calculations by the approximation method on the Bethe lattice in the case of spin-crossover transitions. An increase in the parameter α enlarges the loop with a T_{eq} shifted to lower temperatures as observed in our previous work of Ref. [28]. These phenomena are typical of molecular bistable solids [59] and select SC materials for promising applications eg., for information storage [60–62].

From here on, the relaxation dynamics of metastable states of the system is concerned. In experiments, after an irradiation event that saturates n_{HS}, the relaxation process is visualized at low temperature [63–65]. In the present model, the system's relaxation is simulated at different temperatures at some selected values of γ. The sample size considered is still $L = 100$ and more than ten independent runs are used. Typical one-step relaxation curves are obtained for n_{HS} in Fig. 7. At $T = 18$ K sigmoidal curves are got with one-step relaxation (see Fig. 7a). We are far from the plateau found around $n_{HS} = 0.5$ for $T = 20; 23$ K (see Fig. 7b,c). When $\gamma = 0$, the system lies in the HS state for a long time before starting its relaxation. Things happen as in a supersaturated fluid where fluctuations take long time to create a supercritical nucleus of the new phase. Once over this barrier, a fast exponential decay of the HS state is observed. In this case, molecules pass from HS to LS independently of each other. But for values of nonzero γ, one gets a strongly interacting system. Relaxation curves are self-accelerated in the initial stage of the process and become increasingly steeper. This trend is observed in all panels up to $\gamma = 0.5$. For $\gamma > 0.5$, the relaxation time increases with γ. n_{HS} shows sigmoidal shape and its decay is rather faster than what is found above 18 K. We check that during the relaxation process, most microscopic events are processes that decrease the system energy. Similar trends

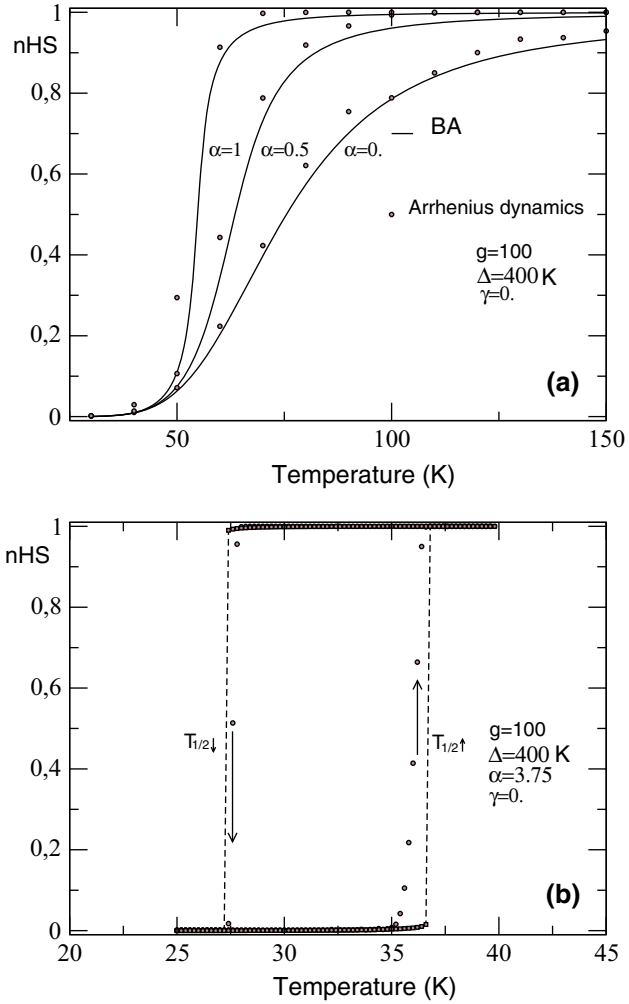

Fig. 6 Compared results of the high-spin fraction n_{HS} calculated by Monte Carlo simulations (MCS) with Arrhenius dynamics (*open circles*) and the Bethe lattice approach (*lines*). In panel (**b**) non-equilibrium hysteresis loop is computed for the parameter values written in the panel using both methods: MCS (*open circles*) and Bethe lattice approach (*diamonds with dashed lines*) in the range of equilibrium temperatures (see text)

are observed at $T = 20$ K and 22 K excepted the existence of a plateau around $n_{HS} = 0.5$ for $\gamma = 0.75$ (Fig. 7b,c). At $T = 20$ K, the plateau is simply a reflection of the downward branch of the hysteresis loop. This is justified by the results displayed in Fig. 8a where the equilibrium temperatures are 29.80 and 20.40 K on upward and downward branches, respectively. Obviously, at $T = 22$ K, we are inside the hysteresis loop and the relaxation time becomes longer than for $\gamma \leq 0.5$.

On the order hand, Nishino et al. [31] explained that the relaxation from the HS–LS to LS state is governed by the nucleation process [36] because HS–LS state is rather strongly metastable. The nucleation of LS units appears stochastically. Accordingly, the relaxation of HS–LS

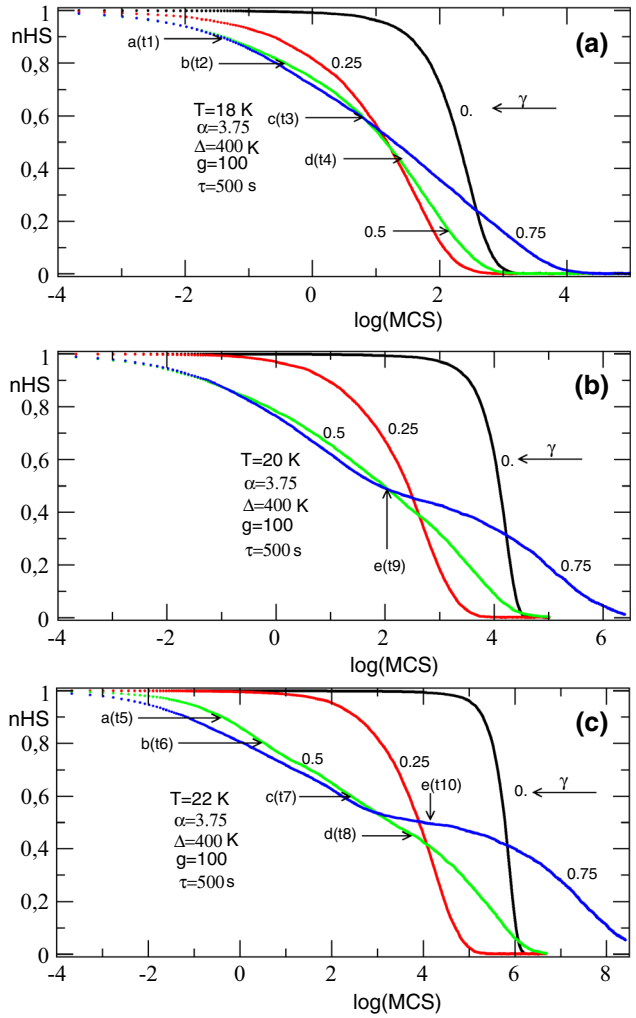

Fig. 7 Relaxation curves from the HS state to the LS state for selected values of γ:0 (*black*); 0.25 (*red*); 0.5 (*green*); 0.75 (*blue*) at different temperatures $T = 18$ K (**a**); $T = 20$ K (**b**) and $T = 22$ K (**c**). In these calculations, $E_0^a = 0$. One can remark a one-step relaxation in all three panels. A plateau in the domain HS–LS for $\gamma = 0.75$ (see panels **b**, **c**) is observed. The length of the plateau in different panels increases in this range of temperature. It is absent in panel (**a**). This plateau where n_{HS} appears almost constant may correspond to situation where HS unit clusters population makes a random work around an average value. The system within the plateau seems to be in a metastable equilibrium state

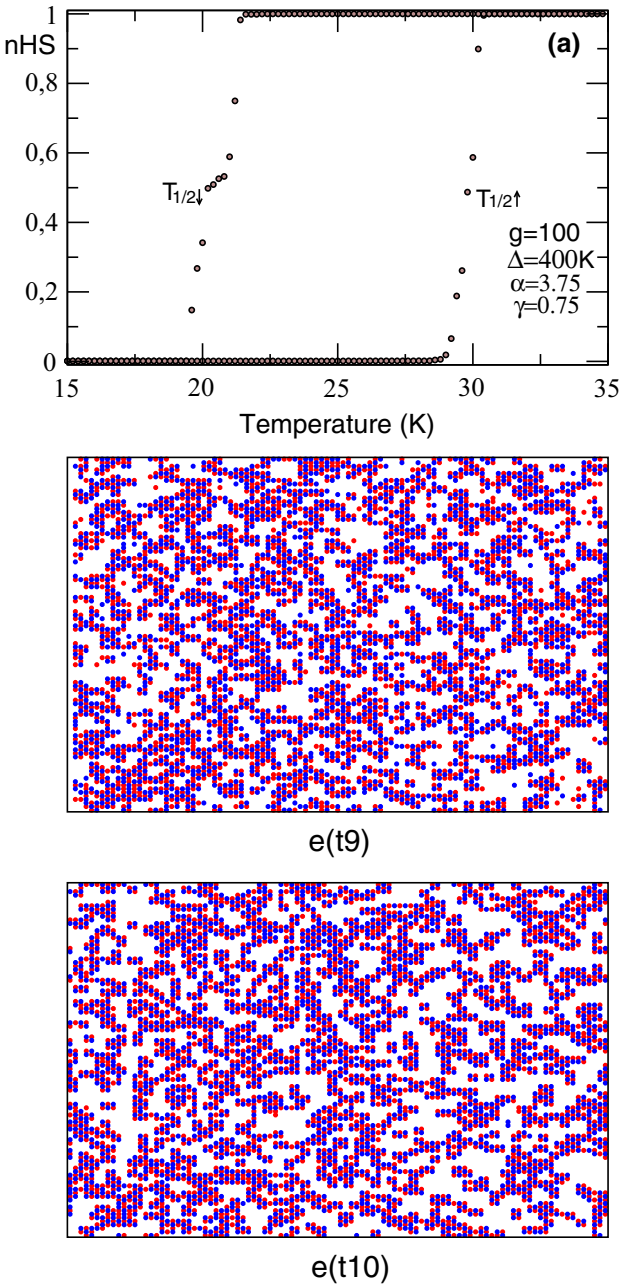

Fig. 8 Thermal non-equilibrium hysteresis loop computed for selected values (*written on the curves*) of the physical parameters using Monte Carlo simulations (**a**). The next panels show snapshots of LS units (*white species*) during the relaxation near the plateau at $T = 20$ K and $T = 22$ K, respectively. *Red* and *blue dots* are associated with HS units with the spin values $+1$ and -1, respectively. Calculations are performed at the times $t_9 = 5.98$ s and $t_{10} = 56.63$ s, respectively, with $E_0^a = 0$ K. Other parameters are $\Delta = 400$ K; $g = 100$; $\gamma = 0.75$ and $\alpha = 3.75$

metastable units should depend on the height of the energy barrier and temperature. For $\gamma = 0.75$, below $n_{HS} = 0.5$, the relaxation speed is accelerated accompanied by slow concave relaxation to the LS phase. It is noticed that the sigmoidal character progressively strengthens with increasing exchange parameter γ. At each inflection point of the curves indicated by e(t_9) and e(t_{10}), the total energy change ΔE is often zero (Fig. 7b,c). The corresponding lattice topographies are obtained at $t_9 = 5.98$ s for $T = 20$ K and at $t_{10} = 56.63$ s for $T = 22$ K (see Fig. 8). The proportion of free intermediate states HS–LS pairs decreases as the temperature increases [50]. It is of the order of 30.83 and 27.53 %, respectively. There, thermal fluctuations act as a driving force for the appearance of the new LS phase. Results are averaged over 20 independent

runs. A rearrangement of the LS units occurs when passing from one temperature to a higher one. A kind of coalescence occurs. So, for the same value of γ, the effect of correlations [66] decreases as the temperature increases in the HS–LS domain. It is very interesting to analyze in the hysteresis loop of Fig. 8a, the behavior of the system during relaxation beyond 22 K. For $\gamma = 0.75$ and other parameters fixed to their previous values, one gets Fig. 9 which shows the behavior of the magnetization m and the fraction n_{HS} at two temperatures: $T = 23$ and 23.5 K. The relaxation process normally occurs as before; only the decay of the magnetization is much faster than for n_{HS} and becomes slower as the temperature increases (see both panels). The plateau always appears and tends to disappear (see panel b) when the temperature approaches $(T_{1/2\downarrow} + T_{1/2\uparrow})/2 = 25.10$ K (Fig. 8a) where the relaxation time is almost infinite, because one is close to the equilibrium temperature at which the free energies of both HS and LS phases are equal. So, this process does not only depend on the height of the energy barrier, but also on the temperature. Hence, the relaxation curves show the typical sigmoidal shape for a cooperative process [31, 35, 67], where the energy barrier progressively decreases, while the relaxation proceeds. As in the thermally activated regime of real spin-crossover complexes, the relaxation from the HS state is faster at higher temperature [50] and for increasing exchange coupling parameter [35] (see Fig. 10).

Figure 11 displays the thermal behavior of the high-spin fraction n_{HS} and the lattice magnetization m as functions of γ for $\alpha = 0.5$ and 3.75, respectively. All other parameters are set to their previous values. For each value of α, n_{HS} curves shifted downwards when γ increases. The opposite occurs with the magnetization. There is a gradual conversion for $\alpha = 0.5$; it becomes quite abrupt for $\alpha = 3.75$.

Figures 12 and 13 display snapshots of the system when subjected to relaxation from HS to LS at $T = 18$ K and $T = 22$ K, respectively. At $T = 18$ K, E_0^a is set to 120 K; $\Delta = 400$ K; $g = 100$; $\alpha = 3.75$ and $\gamma = 0.5$. One gets at time $t_1 = 6.43$ s, 10 % of sparse LS nucleated units. At $T = 22$ K, with E_0^a set to 70 K and other parameters maintained to the previous values, one statistically gets again 10 % of LS nucleated units at $t_5 = 11.36$ s. From Figs. 12a–d and 13a–d, one assists to a kind of a two-dimensional nucleation growth of LS units with the birth and spread of numerous LS supercritical unit clusters. This statement is strengthened by the increase in the size of the small LS unit clusters observed at the initial stage of the

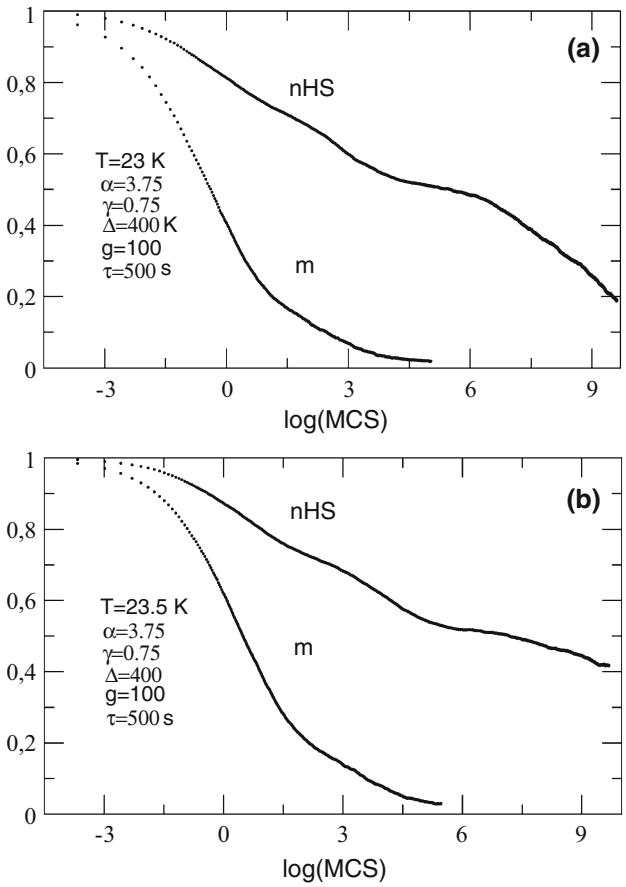

Fig. 9 Relaxation curves from HS state to LS state and the magnetization m within the hysteresis loop for $\gamma = 0.75$ at different temperatures: $T = 23$ K (**a**) and $T = 23.5$ K (**b**). Values of other parameters are written in the panels. On n_{HS} *curves*, one can remark the disappearance of the plateau when the temperature approaches $(T_{1/2\downarrow} + T_{1/2\uparrow})/2 = 25.10$ K (see panel **b**). The relaxation of the magnetization m is faster than for n_{HS}

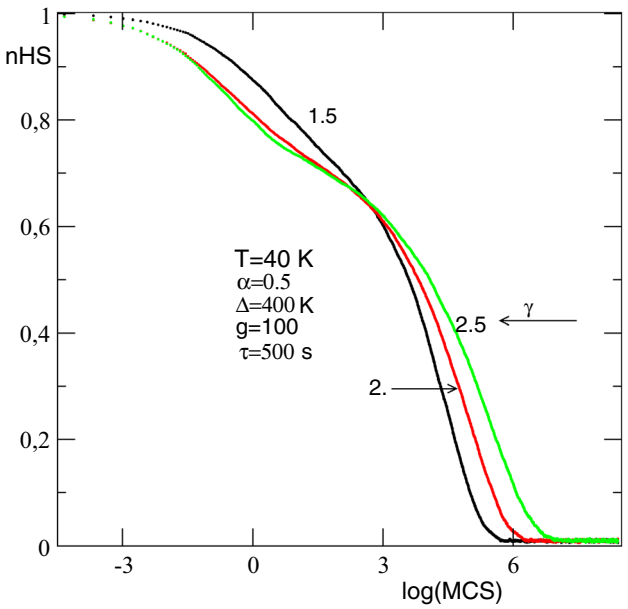

Fig. 10 Relaxation curves from the HS state to the LS state at high temperature for selected values of γ: 1.5 (*black*); 2. (*red*) and 2.5 (*green*) at fixed value of α (= 0.5). The relaxation proceeds normally as observed in Fig. 7 but here, the relaxation times are slightly reduced [63]

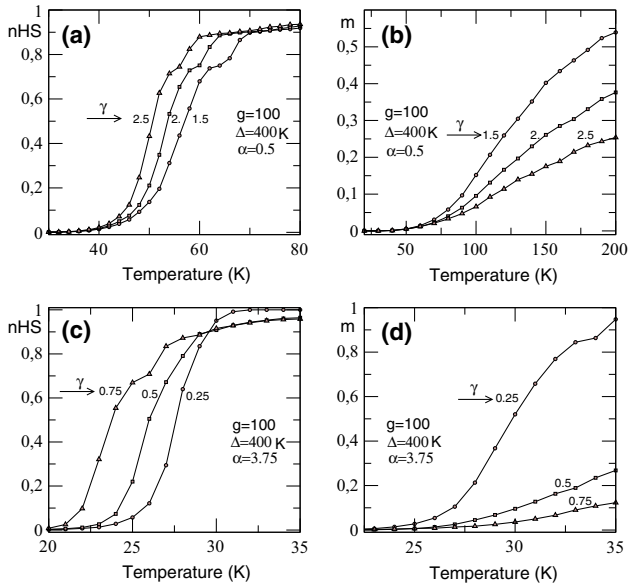

Fig. 11 Thermal behaviors of the high-spin fraction n_{HS} (panels **a**, **c**) and the magnetization m (panels **b**, **d**) at some selected values of γ: 1.5; 2.; 2.5 and 0.25; 0.5; 0.75 for $\alpha = 0.5$ and $\alpha = 3.75$ respectively. For increasing temperature T and magnetic interactions γ, n_{HS} curve shifts to the *left* whereas the curve of the magnetization m decreases and shifts to the *right*. In the panels **a** and **b**, gradual conversion occurs but in other panels the transition is first order (see text). Values of other parameters are written in the panels

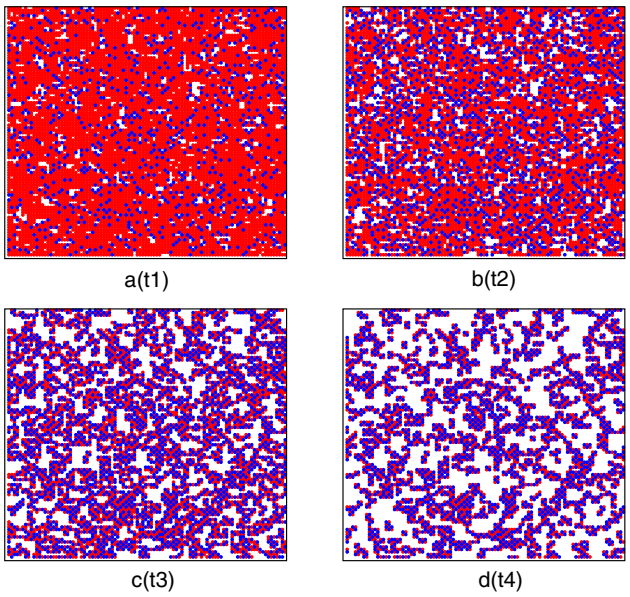

Fig. 12 Snapshots of system configuration at $T = 18$ K at different relaxation times: $t_1 = 6.43$ s; $t_2 = 15.70$ s; $t_3 = 184.00$ s and $t_4 = 686.34$ s. White clusters correspond to those of LS units whereas the *red* (spin $+1$) and *blue* (spin -1) *dots* consist of HS unit clusters. As it appears evident, n_{LS} increases in the course of the time. In **a**, **b**, **c** and **d**, respectively, 10, 20, 40 and 55 % of the lattice are occupied by LS units. Values considered for other parameters are: $\Delta = 400$ K; $g = 100$; $\alpha = 3.75$; $\gamma = 0.5$ and $E_0^a = 120$ K

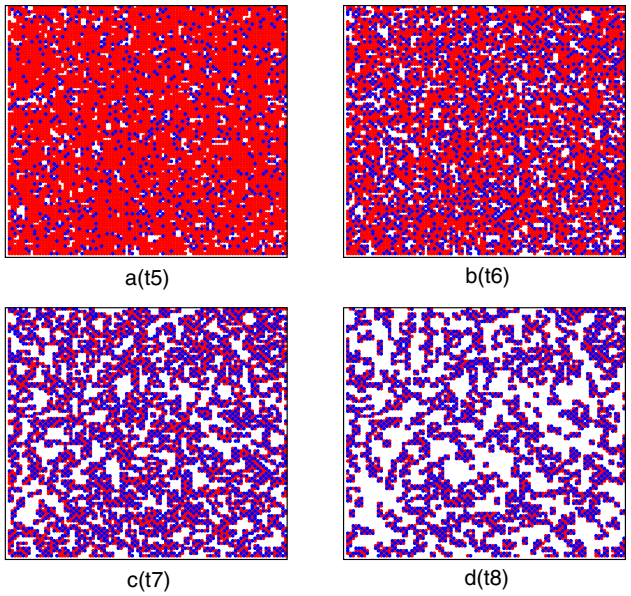

Fig. 13 Snapshots of the system configuration at $T = 22$ K at different relaxation times: $t_5 = 11.36$ s ; $t_6 = 28.73$ s; $t_7 = 330.09$ s; $t_8 = 1277.34$ s. Corresponding percentages of LS units are also: 10 % (**a**); 20 % (**b**); 40 % (**c**); 55 % (**d**). Values considered for other model parameters are: $\Delta = 400$ K; $g = 100$; $\alpha = 3.75$; $\gamma = 0.5$ and $E_0^a = 70$ K. *Colors* have the same meaning as in Fig. 12

relaxation process. The number of particles switching within a given time interval increases since more and more molecules populate the LS state. That is the basic mechanism for the self-accelerated relaxation [55]. Such phenomenon also called cooperativity is observed in several spin-crossover systems [31].

Two interacting remarks emerge. The first one concerns the relaxation time. At small thermal fluctuations (Fig. 7a), all relaxation curves converge and relaxation times remain almost unchanged although relaxation paths are initially different, excepted for $\gamma \geq 0.75$. The relaxation time appears to be independent of γ as long as thermal fluctuations are limited. Second, in Figs. 7b,c the relaxation curves change trend for nonzero value of γ at about $n_{\mathrm{HS}} = 0.5$ with a plateau. The shape of the relaxation curves is then influenced by the magnetic interaction parameter γ. Moreover, the temperature is an important factor in this range. The plateau appears and becomes stressed. More calculations are certainly necessary to understand these different findings and to check wether the present relaxation dynamics can be fully described within the $2D$-nucleation theory.

4 Conclusion

Static and dynamical properties of SC and PBA materials have been phenomenologically addressed in this work. Two methods are used: Monte Carlo simulations with

Arrhenius dynamics and the Bethe lattice approach. Both methods yield results that are in agreement with those from Ref. [28] concerning the high-spin fraction and different phase transitions. When the magnetic interactions are weak, the only one transition observed is the diamagnetic–paramagnetic transition. It becomes of first order when the spin–phonon interaction becomes important. By the Bethe approximation method, the only one difference observed is that the critical temperatures are slightly lower with respect to those by CEFT calculations [28].

In the dynamical case, an hysteresis loop at the vicinity of the first-order transition is obtained. We have studied the relaxation from the fully saturated non-equilibrium HS state for weak magnetic interactions and at relatively low temperatures. This simulates the relaxation from the photo-excited saturated high-spin state. It is found that the relaxation of the HS fraction is of two types. First, fast relaxation from HS to HS–LS state occurs for increasing magnetic interactions. The initial sigmoidal shape due to Arrhenius transition probabilities in the Monte Carlo simulations that is typical for spin-crossover compounds is recovered. A slow relaxation follows from the HS–LS to LS state. Second, at low temperature, the relaxation occurs for a too long duration time, and a plateau appears in the HS–LS domain. LS unit clusters are formed and get bigger. These clusters later coalesce as in a two-dimensional nucleation mechanism. The study of the statistics of LS species and aggregates in the model parameters' space may help to understand the key growth mechanisms that occur during the decay of the metastable HS state. Beyond that, it will be interesting to study the system dynamics relying on the free energy dynamics. Indeed, writing $\frac{\mathrm{dm}}{\mathrm{d}t} = -\frac{\partial F(m,q)}{\partial m}$ and $\frac{\mathrm{dq}}{\mathrm{d}t} = -\frac{\partial F(m,q)}{\partial q}$, where F denotes the free energy of the system [67], new interesting developments leading to novel properties of the SC materials can be obtained.

References

1. P. Gütlich, Harold A. Goodwin, *Spin-Crossover in Transition Metal Compounds I, II and III* (Springer, Berlin, 2004)
2. J.H. Ammeter, Nouv. J. Chim. **4**, 631 (1980)
3. S. Ohkoshi, K. Hashimoto, J. Am. Chem. Soc. **121**, 10591 (1999)
4. S. Ohkoshi, S. Ikeda, T. Hozumi, T. Kashiwagi, K. Hashimoto, J. Am. Chem. Soc. **128**, 5320 (2006)
5. S. Ohkoshi, K. Imoto, Y. Tsunobuchi, S. Takano, H. Tokoro, Nat. Chem. **3**, 564 (2011). doi:10.1038/nchem.1067
6. D.A. Pejakovíc, J.L. Manson, C. Kitamura, J.S. Miller, A.J. Epstein, Polyhedron **20**, 1435 (2001)
7. H. Tokoro, S-i Ohkoshi, K. Hashimoto, Appl. Phys. Lett. **82**, 1245 (2003)
8. K. Kato, Y. Moritomo, M. Takata, M. Sakata, M. Umekawa, N. Hamada, S. Ohkoshi, H. Tokoro, K. Hashimoto, Phys. Rev. Lett. **91**, 255502 (2003)
9. A. Gîndulescu, A. Rotaru, J. Linares, M. Dimian, J. Nasser, J. Phys. Conf. Ser. **268**, 012007 (2011)
10. M. Sorai, S. Seki, J. Phys. Chem. Solids **35**, 555 (1974)
11. M.A. Halcrow, *Spin-Crossover Materials: Properties and Applications* (Wiley, New York, 2013)
12. P. Gütlich, A.B. Gaspar, Y. Garcia, Beilstein J. Org. Chem. **9**, 342 (2013)
13. C.M. Quintero, G. Félix, I. Suleimanov, J.S. Costa, G. Molnár, L. Salmon, W. Nicolazzi, A. Bousseksou, Beilstein J. Nanotechnol. **5**, 2230 (2014)
14. E. König, Struct. Bond **76**, 51 (1991)
15. J. Wajnflasz, Phys. Status Solidi B **40**, 537 (1970)
16. M. Nishino, S. Miyashita, K. Boukheddaden, J. Chem. Phys. **118**, 4594 (2003)
17. Iu Gudyma, V. Ivashko, J. Linares, J. Appl. Phys. **116**, 173509 (2014)
18. J.A. Nasser, Eur. Phys. J. B **21**, 3–10 (2001)
19. K. Boukheddaden, M. Nishino, S. Miyashita, Phys. Rev. B **75**, 094112 (2007)
20. H. Spiering, N. Willenbacher, J. Phys, Condens. Matter **1**, 10089 (1989)
21. A. Rotaru, J. Linares, E. Codjovi, J. Nasser, A. Stancu, J. Appl. Phys. **103**, 07B980 (2008)
22. A. Rotaru, A. Camona, F. Combaub, J. Linares, A. Stancu, J. Nasser, Polyhedron **28**, 1684 (2009)
23. A. Slimani, K. Boukheddaden, F. Varret, M. Nishino, S. Miyashita, J. Chem. Phys. **139**, 194706 (2013)
24. A. Slimani, K. Boukheddaden, F. Varret, H. Oubouchou, Phys. Rev. B **87**, 014111 (2013)
25. Iu Gudyma, A. Maksymov, C. Enachescu, Phys. Rev. B **89**, 224412 (2014)
26. K. Boukheddaden, M. Nishino, S. Miyashita, PRL **100**, 177206 (2008)
27. K. Boukheddaden, S. Miyashita, M. Nishino, F. Varret, Phys. Rev. B **72**, 014467 (2005)
28. T.D. Oke, F. Hontinfinde, K. Boukheddaden, Eur. Phys. J. B **86**, 271 (2013)
29. S. Jain, *Monte Carlo Simulations of Disordered Systems* (World Scientific Publishing Co., Pte. Ltd, Singapore, 1992)
30. K. Binder, D.W. Heermann, *Monte Carlo Simulation in Statistical Physics*, 5th edn. (Springer, Berlin Heidelberg, 2010). doi:10.1007/978-3-642-03163-2
31. M. Nishino, K. Boukheddaden, S. Miyashita, F. Varret, Phys. Rev. B **68**, 224402 (2003)
32. M. Nishino, K. Boukheddaden, S. Miyashita, F. Varret, Polyhedron **24**, 2852 (2005)
33. K. Boukheddaden, I. Shteto, B. Hôo, F. Varret, Phys. Rev. **62**, 14796 (2000)
34. K. Boukheddaden, Phys. Rev. **62**, 14806 (2000)
35. S. Mouri, K. Tanaka, S. Bonhommeau, N.O. Moussa, G. Molàr, A. Bousseksou, Phys. Rev. B **78**, 174308 (2008)
36. M. Nishino, C. Enachescu, S. Miyashita, Per Anne Rikvold, K. Boukheddaden, F. Varret, Sci. Rep. (2011). doi:10.1038/srep00162
37. A. Povilus, Physics 441-Fall (2003)
38. O. Sato, T. Iyoda, A. Fujishima, K. Hashimoto, Science **272**, 704 (1996)
39. O. Sato, Y. Einaga, T. Iyoda, A. Fujishima, K. Hashimoto, J. Electrochem. Soc. **144**, L11 (1997)
40. S-i Ohkoshi, Y. Abe, A. Fujishima, K. Hashimoto, Phys. Rev. Lett. **82**, 1285 (1999)
41. T. Matsuda, H. Tokoro, K. Hashimoto, S. Ohkoshi, Dalton Trans. **2006**, 5046 (2006)
42. M. Itoi, I. Maurin, F. Varret, F.A. Frye, D.R. Talham, D. Chernyshov, K. Boukheddaden, Phys. Rev. B **88**, 094104 (2013)
43. C. Domb, Adv. Phys. **9**, 208 (1960)

44. C.K. Hu, NSh Ismailian, K.B. Oganesyan, Phys. Rev. E **59**, 6489 (1999)
45. B.D. Hughes, M. Sahimi, Phys. Status Solidi B **29**, 781 (1982)
46. R.J. Baxter, *Exactly Solvable Models in Statistical Mechanics* (Academic Press, New York, 1982)
47. E. Albayrak, A. Yigit, Phys. Lett. A **353**, 121 (2006)
48. E. Albayrak, M. Keskin, J. Magn. Magn. Mater. **241**, 249 (2002)
49. A.Z. Akheyan, N.S. Ananikian, J. Phys. A Math. Gen. **29**, 721 (1996)
50. K. Boukheddaden, Eur. J. Inorg. Chem. doi:10.1002/ejic.201201093
51. C. Enachescu, M. Nishino, S. Miyashita, A. Hausser, A. Stancu, L. Stoleriu, EPL **91**, 27003 (2010)
52. C. Enachescu, L. Stoleriu, A. Stancu, Phys. Rev. Lett. **102**, 257204 (2009)
53. P. Gütlich, A. Hausser, H. Spiering, Angew. Chem. **33**, 2024 (1994)
54. S.W. Biernacki, B. Clerjaud, Phys. Rev. B **72**, 024406 (2005)
55. K. Boukheddaden, J. Linares, H. Spiering, F. Varret, Eur. Phys. J. B **15**, 317 (2000)
56. S. Miyashita, Y. Konishi, H. Tokoro, M. Nishino, K. Boukheddaden, F. Varret, Prog. Theor. Phys. **114**, 719 (2005)
57. S. Miyashita, M. Nishino, Y. Konishi, H. Tokoro, K. Boukheddaden, F. Varret, Per Arne Rikvold, J. Phys. Conf. Ser. **148**, 012027 (2009)
58. Gabriele D'Avino, Anna Painelli, K. Boukheddaden, Phys. Rev. B **84**, 104119 (2011)
59. K. Boukheddaden, J. Linares, E. Codjovi, F. Varret, V. Niel, J.A. Real, J. Appl. Phys. **93**, 7103 (2003)
60. O. Kahn, *Molecular Magnetism* (VCH, New York, 1993)
61. O. Kahn, J. Krober, C. Jay, Adv. Mater. Weinheim, Germany **11**, 4 (1992)
62. E. Freysz, S. Montant, S. Létard, J.-F. Létard, Chem. Phys. Lett. **394**, 318 (2004)
63. Y. Ogawa, T. Ishikawa, S. Koshihara, K. Boukheddaden, F. Varret, Phys. Rev. B **66**, 073104 (2002)
64. A. Hausser, Coord. Chem. Rev. **111**, 275 (1991)
65. F. Varret, K. Boukheddaden, C. Chong, A. Goudjon, B. Gillon, J. Jeftic, A. Hausser, Eur. Phys. Lett. **77**, 30007 (2007)
66. H. Spiering, T. Kohlhaas, H. Romstedt, A. Hausser, C. Bruns-Yilmaz, J. Kusz, P. Gütlich, Coord. Chem. Rev. **190**, 629 (1999)
67. M. Nishino, K. Boukheddaden, S. Miyashita, F. Varret, Phys. Rev. B **72**, 064452 (2005)